Analysis of thermocline thermal energy storage systems with generic initial condition algebraic model

Aristides M. Bonanos [*], Evgeny V. Votyakov

Energy Environment and Water Research Center, The Cyprus Institute, Nicosia 2121, Cyprus

A B S T R A C T

Thermal energy storage is key in making solar-thermal power plants more economically competitive compared to conventional plants. In this work, a new algebraic solution for thermocline thermal energy storage tanks, allowing for any initial temperature profile, is developed and presented. The model, called the Algebraic IC model, is successfully validated by comparing with experimental data and numerical solution of the governing partial differential equations. Additionally, the algebraic solution is extended to incorporate heat losses from the thermocline tank walls to the environment. The algebraic solution is significantly less computationally expensive than other one-dimensional models, since algebraic, rather than differential, equations are solved. An explicit formula for optimal fluid velocity is developed and validated through a parametric study of a thermocline tank. The effect of the dimensionless heat transfer coefficient is also investigated. Finally, the operation of thermocline tanks under multiple consecutive charging and discharging cycles is studied. The tank efficiency depends on the amount of thermocline allowed to exit during each cycle, and was found to decrease initially and subsequently reach steady state in less than 10 cycles.

1. Introduction

Renewable energy sources will increasingly contribute to the future energy mix, particularly in the context of the European Green Deal on net carbon emission neutrality by 2050 and similar global initiatives aiming to mitigate climate change. However, the intermittent nature of most renewable resources necessitates coupling them with energy storage solutions to match demand with supply.

Concentrating solar thermal power is readily coupled with thermal energy storage solutions, allowing for clean and dispatchable renewable energy. Thermal energy storage offers several advantages over mechanical or chemical storage, such as lower capital cost and high efficiency (Kuravi et al., 2013). In the present work, we consider sensible thermal energy storage and specifically the packed-bed thermocline single-tank storage solution. In this solution, a single tank is used with hot and cold fluid separated by natural stratification. A temperature gradient, also called the thermocline, separates the hot and cold regions. As energy is added or removed from the tank during charging or discharging, the thermocline moves within the tank, with the typical operation described in Section 2.

In the past years, several works report on numerical investigations

relating to the use of thermoclines as storage solutions for concentrating solar thermal power applications. These works vary in complexity and detail, and may be classified in terms of the dimensionality of the equations solved. The most detailed consider the full three-dimensional equations of motion, solving coupled conservation equations for mass momentum and energy (Yang and Garimella, 2010; Xu et al., 2012; Flueckiger et al., 2011; Flueckiger and Garimella, 2012), while others assume one-dimensional flow allowing for solution of only the energy equation (Van Lew et al., 2011; Xu et al., 2012; Bayon and Rojas, 2013). Despite the greater detail and information obtained from the three-dimensional studies, these results are difficult to validate due to lack of detailed experimental data. Indeed, the experimental data typically available consists of the thermocline evolution over time (Pacheco et al., 2002; Hänchen et al., 2011; Bruch et al., 2014; Hoffmann et al., 2016; Bayon and Rojas, 2018), which can be described very well by the reduced order e.g. one-dimensional) models.

Reduced order models have been used to study the integration of thermocline storage in CST plants, specifically operational challenges and characteristics arising from the use of this type of storage. The storage efficiency, and hence electricity production, of a thermocline system will be lower than that of a two-tank design, because of thermocline degradation over time. Here, thermocline degradation refers to

---

Nomenclature

A	Specific surface area [m^2/m^3]	β	ratio of thermal conductivity to effective thermal conductivity
Bi	Biot number	γ	ratio of volumetric heat capacity to effective volumetric heat capacity
C_p	Heat capacity [J/kg K]	ε	Void fraction
$D^\star$	Dimensionless diffusion coefficient	ζ	Non-dimensional spatial coordinate
d_p	Particle diameter [m]	η	Tank efficiency
h	Heat transfer coefficient [W/m^2 K]	θ	Non-dimensional temperature
k	Thermal conductivity [W/m K]	λ	Thermocline thickness
L	Tank height [m]	μ	Mean of elementary effects in OAT screening method
Nu	Nusselt number	ν	Kinematic viscosity [m^2/s]
Pe	Peclet number	ρ	Density [kg/m^3]
Pr	Prandtl number	σ	Standard deviation of elementary effects in OAT screening method
R	Tank radius [m]		
Re	Reynolds number	τ	Non-dimensional time
S, S_T	Sensitivity index and Total sensitivity index for variance based sensitivity analysis	ω	Transformed coordinate for Algebraic IC solution
T	Temperature [°C]	*Subscripts*	
t	Time [s]	*amb*	Ambient condition
u	Fluid velocity [m/s]	∞	Cold condition
$u^\star$	Non-dimensional velocity	eff	Effective property
z	Spatial coordinate [m]	f	Fluid property
		in	Hot condition
Greek		s	Solid filler property
α	Thermal diffusivity	w	Wall property

the thickening of the temperature transition zone defining the thermocline. This effect can be mitigated by appropriate operational strategies during charging and discharging cycles, such as total or partial extraction of the thermocline region (Biencinto et al., 2014). Further, due to the temperature cycling, the tank walls and solid filler materials expand at different rates, potentially leading to tank failure from thermal ratcheting as the filler settles. In a study of the Solar One facility, thermal ratcheting was found not to be an issue, although those findings had a large uncertainty (Faas et al., 1986). Other studies propose to decrease the ratcheting effect through design or operational strategies, by increased fluid velocity (Wang et al., 2020), or changing thermocline tank porosity, filler material selection, and tank insulation (Flueckiger et al., 2011; Wang et al., 2020).

Regarding the development of reduced order models, the work of the current authors is highlighted (Votyakov and Bonanos, 2014, 2015; Bonanos and Votyakov, 2016). In this series of manuscripts, the authors present an appropriate dimensionless form of the governing equations, enabling direct comparison of multiple designs, and develop an algebraic model that approximates the solution of the two-phase one-dimensional unsteady energy equations for packed-bed thermocline tanks (c.f. Eq. (1)). The solution of the two-phase one-dimensional model involves the error function, so the authors demonstrated that the use of an analytical approximation to it is suitable, allowing for an explicit expression for the thermocline thickness as a function dimensionless parameters to be obtained. This expression allows to make a rough assessment of the storage efficiency without any simulations, based only on the material and operation properties. Further, an algebraic relation between the fluid and solid materials is developed, allowing for recovery of both temperature fields, and thus overcoming a weakness of other one-dimensional single-phase models.

In the present study, we extend the algebraic model of Votyakov and Bonanos (2014, 2015) to accommodate a non-uniform tank temperature as an initial condition to the model and to include effects of thermal losses from the tank walls to the environment. This was done to extend the generality of the model, but also to better match the initial temperature profiles observed in several experimental studies, such as in Pacheco et al. (2002), Hänchen et al. (2011), and Hoffmann et al. (2016)

to cite a few. Additionally, even if a thermocline tank starts at uniform temperature, after multiple charging and discharging cycles with incomplete thermocline extraction, the starting profile for all subsequent cycles after the first will no longer be a step function. We demonstrate how the algebraic model can be used to predict the optimal tank charging/discharging velocity and therefore govern tank sizing. Finally, using the newly developed initial conditions, the behavior of thermocline tanks under multiple cyclical charging and discharging cycles is studied.

The structure of this article is as follows: in Section 2, the existing algebraic model is reviewed and subsequently the new Algebraic IC is derived, for arbitrary initial temperature distribution and inclusion of thermal losses from the thermocline tank walls. In Section 3, the model is validated against a recent experimental study, highlighting its range of applicability and accuracy. In Section 4, the new model is used to study the impact fluid velocity and thermal losses on the thermocline, as well as the behavior of such a storage tank under consecutive cycle operation, and we conclude with a summary of the findings.

2. Model development

The packed-bed thermocline tank description has been given elsewhere (Yang and Garimella, 2010; Flueckiger et al., 2013; Votyakov and Bonanos, 2014, 2015; Bonanos and Votyakov, 2016; Esence et al., 2017), however the main elements of the operation and mathematical model is repeated here for completeness.

The general layout of a thermocline storage system is presented in Fig. 1, and is similar to that used by others (Xu et al., 2012; Yang and Garimella, 2010). The storage volume, with height L, consists of a cylindrical tank packed with small solid particles, called the filler material. A heat transfer fluid, referred to as fluid herein, enters the storage tank through a distributor and circulates in the tank transferring heat to the filler material. The role of the distributor is to ensure a uniform radial velocity; however in the current work this flow distribution is not modeled, rather assumed to be uniform, allowing for only one spatial dimension to be considered. The volume fraction of the fluid compared over the overall tank volume is defined as the void fraction, ε. During a
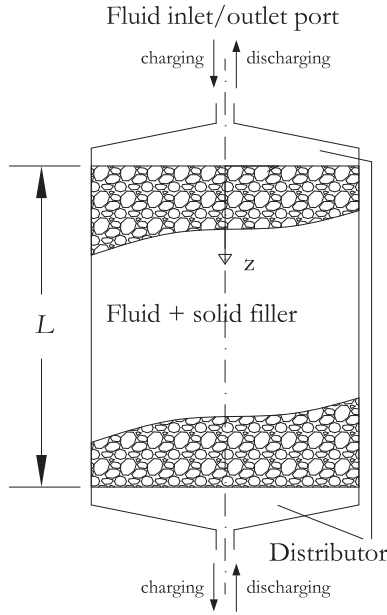
Fluid inlet/outlet port

Fig. 1. Schematic of a packed-bed thermocline thermal storage tank.

charging cycle, the tank is initially at a cold temperature, T_∞, and hot fluid at temperature T_{in} enters from the top of the tank, heating the filler material, and exits at a temperature $\geqslant T_\infty$. In the following discharge cycle, cold fluid enters from the bottom of the tank and the process is reversed.

Such systems are typically modeled with the transient, one-dimensional, two-phase, volume averaged energy equations, for the fluid and solid filler, respectively, as:

$$\varepsilon(\rho C_p)_f \frac{\partial T_f}{\partial t} + \varepsilon(\rho C_p)_f u \frac{\partial T_f}{\partial z} = k_{f,\text{eff}}\left(\frac{\partial^2 T_f}{\partial z^2}\right) + h_{sf} A_{sf}(T_s - T_f) + h_w A_w(T_{amb} - T_f),$$

$$(1-\varepsilon)(\rho C_p)_s \frac{\partial T_s}{\partial t} = k_{s,\text{eff}}\left(\frac{\partial^2 T_s}{\partial z^2}\right) - h_{sf} A_{sf}(T_s - T_f).$$
(1)

Here, the term $h_w A_w(T_{amb} - T_f)$ represents thermal losses from the tank wall to ambient conditions. In the current section this term is neglected, but the solution including thermal losses is addressed in Section 2.3.

For the fluid-to-solid heat transfer coefficient, h_{sf}, the following Nusselt correlation is used (Wakao and Funazkri, 1978; Wakao et al., 1979; Amiri and Vafai, 1994),

$$\text{Nu} = \frac{h d_p}{k} = 2 + 1.1 \, \text{Pr}^{1/3} \, \text{Re}^{0.6},$$
(2)

where $\text{Re} = u d_p/\nu_f$ and $\text{Pr} = \nu_f(\rho C_p)_f/k_f$, for $15 \leqslant \text{Re} \leqslant 8500$. The filler material particle diameter, d_p, is small compared to the tank dimensions; indicatively, for quartzite rock as the filler material, particle diameters are $< 0.1\,\text{m}$ (Yang and Garimella, 2010; Bruch et al., 2014).

The specific surface area of the packed bed, A_{sf}, is derived based on geometrical considerations and is given as (Vafai and Sozen, 1990; Kuznetsov, 1995):

$$A_{sf} = \frac{6(1-\varepsilon)}{d_p}.$$
(3)

When considering porous media, it is convenient to define "effective" transport properties as:

$$\Phi_{f,\text{eff}} = \varepsilon \Phi_f, \Phi_{s,\text{eff}} = (1-\varepsilon)\Phi_s, \Phi_{\text{eff}} = \Phi_{f,\text{eff}} + \Phi_{s,\text{eff}},$$
(4)

where Φ is any intrinsic property, such as thermal conductivity, k, or thermal diffusivity, $\alpha = k/(\rho C_p)$, etc.

2.1. Algebraic model

By using the non-dimensional parameters:

$$\theta = \frac{T - T_\infty}{T_{in} - T_\infty}, \tau = \frac{t \alpha_{\text{eff}}}{L^2}, \zeta = z/L,$$
(5)

and introducing the following material- and flow-related parameters:

$$\beta_f = \frac{\varepsilon k_f}{k_{\text{eff}}}, \beta_s = \frac{(1-\varepsilon)k_s}{k_{\text{eff}}}, \gamma_f = \frac{\varepsilon(\rho C_p)_f}{(\rho C_p)_{\text{eff}}}, \gamma_s = \frac{(1-\varepsilon)(\rho C_p)_s}{(\rho C_p)_{\text{eff}}}$$

$$\text{Pe} = \frac{uL(\rho C_p)_{\text{eff}}}{\varepsilon k_{\text{eff}}} = \text{RePr}\frac{\beta_f}{\varepsilon \gamma_f}\frac{L}{d_p}, \text{Bi} = \frac{6(1-\varepsilon)k_f Nu L^2}{k_{\text{eff}} d_p^2},$$
(6)

the two-phase energy equations can be re-cast in dimensionless form as:

$$\gamma_f \frac{\partial \theta_f}{\partial \tau} + \gamma_f \text{Pe} \frac{\partial \theta_f}{\partial \zeta} = \beta_f \frac{\partial^2 \theta_f}{\partial \zeta^2} + \text{Bi}(\theta_s - \theta_f)$$

$$\gamma_s \frac{\partial \theta_s}{\partial \tau} = \beta_s \frac{\partial^2 \theta_s}{\partial \zeta^2} - \text{Bi}(\theta_s - \theta_f)$$
(7)

The above equations were reduced to a single-phase, one-dimensional, transient model (Votyakov and Bonanos, 2014) using perturbation theory, which allows for the fluid temperature to be solved from a differential equation whereas the solid temperature is then obtained through an algebraic equation. The perturbation model is given by:

$$\frac{\partial \theta}{\partial \tau} + \gamma_f \text{Pe} \frac{\partial \theta}{\partial \zeta} = \left(1 + \frac{(\gamma_s \gamma_f \text{Pe})^2}{\text{Bi}}\right)\frac{\partial^2 \theta}{\partial \zeta^2} = D^\star \frac{\partial^2 \theta}{\partial \zeta^2},$$

$$\theta_s = \theta_f + \frac{\gamma_f \gamma_s \text{Pe}}{\text{Bi}}\frac{\partial \theta_f}{\partial \zeta}$$
(8)

An algebraic approximation to the perturbation model was found (Votyakov and Bonanos, 2015), where both fluid and solid temperatures are obtained through algebraic equations, reducing dramatically the solution complexity and time. Substituting $u^\star = \gamma_f \text{Pe}$, the algebraic solution to Eq. (7) is:

$$\theta_f(\tau, \zeta) = \frac{1}{2}\left\{1 \pm \text{erf}\left(\frac{\zeta - u^\star \tau}{\sqrt{4 D^\star \tau}}\right)\right\},$$

$$\theta_s(\tau, \zeta) = \theta_f(\tau, \zeta) + \frac{u^\star \gamma_s}{\text{Bi}}\frac{\partial \theta_f}{\partial \zeta},$$
(9)

where the $-$ sign is for charging and $+$ for discharging, and erf is the error function. A convenient approximation to the latter, with precision greater than $3 \cdot 10^{-3}$, is:

$$\text{erf}(x) = \text{sign}(x)\left[1 - \exp(-4x^2/\pi)\right]^{0.5}.$$
(10)

Further details for the development of these models may be found in (Votyakov and Bonanos, 2014; Votyakov and Bonanos, 2015; Bonanos and Votyakov, 2016). Herein, Eq. (9) with the error function approximation substitution is referred to as the Algebraic Model.

2.2. Generic initial condition

The Algebraic Model was developed for a constant temperature initial condition, e.g. $\theta_f(0, \zeta) = $ constant. However, considering various experimental works, such as (Pacheco et al., 2002; Hänchen et al., 2011; Bruch et al., 2014; Hoffmann et al., 2016), it is evident that the experimentally measured temperature profile at the beginning of the process is not uniform over the length of the tank. This leads to a "lag" of the predicted temperature distribution as compared to the experimental data and to under-predicting the thermocline thickness.

To address this issue, we consider an arbitrary initial condition represented as a polynomial series:

$$\theta_{f,IC}(0,\zeta) = C_0 + C_1\zeta^1 + C_2\zeta^2 + \ldots = \sum_{i=0}^{n} C_i\zeta^i, \tag{11}$$

with the coefficients C_i obtained through fitting an experimental profile. A polynomial was chosen, as it can provide an excellent fit to any experimental profile, given a large enough degree N. We wish to find the solution $\theta_f^{(k)}(\tau,\zeta)$ satisfying Eq. (8) at any $\theta_{f,IC}^{(k)}(\zeta) = \zeta^k$. Then, the full polynomial series solution will be given as:

$$\theta_f(\tau,\zeta) = C_0\theta_f^{(0)}(\tau,\zeta) + C_1\theta_f^{(1)}(\tau,\zeta)\zeta^1 + C_2\theta_f^{(2)}(\tau,\zeta)\zeta^2 + \ldots, \tag{12}$$

Note that if the initial temperature profile is a 0-degree polynomial (e.g. $\theta_f(0,\zeta)=1$: a step function), the solution of Eq. (9) is recovered.

By using Laplace transforms, the solution to an exponential initial condition $\theta_{f,IC}^{exp}(0,\zeta,\alpha) = \exp(\alpha\zeta)$ is found as:

$$\theta_f^{exp}(\tau,\zeta,\alpha) = \frac{1}{2}\left\{1 + \mathrm{erf}\left[\frac{\zeta - u^\star\tau}{\sqrt{4D^\star\tau}} + \alpha\sqrt{D^\star\tau}\right]\right\}\exp\left(\alpha(\zeta - u^\star\tau) + \alpha^2 D^\star\tau\right) \tag{13}$$

A key point in the development of the solution with polynomial series initial conditions, is to observe that:

$$\frac{d}{d\alpha}\exp(\alpha\zeta)\bigg|_{\alpha=0} = \frac{d}{d\alpha}\theta_{f,IC}^{exp}(\zeta,\alpha)\bigg|_{\alpha=0} = \zeta, \tag{14}$$

and so for the kth derivative:

$$\frac{d^k}{d\alpha^k}\exp(\alpha\zeta)\bigg|_{\alpha=0} = \frac{d^k}{d\alpha^k}\theta_{f,IC}^{exp}(\zeta,\alpha)\bigg|_{\alpha=0} = \zeta^k. \tag{15}$$

This allows for starting from the Laplace transform solution for $\theta_f^{exp}(\tau,\zeta,\alpha)$ – Eq. (13) – to obtain the kth solution through k times differentiation of $\theta_f^{exp}(\tau,\zeta)$ as:

$$\theta_f^{(k)}(\tau,\zeta) = \frac{d^k}{d\alpha^k}\theta_f^{exp}(\tau,\zeta,\alpha)\bigg|_{\alpha=0}. \tag{16}$$

To recover the final solution, we introduce the convenient transformations: $\zeta_c = z - u^\star\tau, \lambda = \sqrt{4D^\star\tau}$ and $\omega = \zeta_c/\lambda$. Further, we define the function $f^{(kn)}(x)$ as:

$$f^{(kn)}(\omega) = \begin{cases} \dfrac{1}{2}[1 - \mathrm{erf}(\omega)] = \mathrm{EF}(\omega) & \text{if } k \text{ is even,} \\ \dfrac{1}{\sqrt{\pi}}\exp(-\omega^2) = \mathrm{GF}(\omega) & \text{if } k \text{ is odd.} \end{cases} \tag{17}$$

Therefore, the final form of the algebraic solution with an initial condition being a polynomial temperature profile of Nth degree, hence referred to as Algebraic IC model, is

$$\theta_f(\tau,\zeta) = \theta_f^{(0)}(\tau,\zeta) + \sum_{n=0}^{N}\left[C_n\left(\frac{\lambda}{2}\right)^n\sum_{k=0}^{n}A^{(kn)}\omega^k f^{(kn)}(\omega)\right], \tag{18}$$

where $\theta_f^{(0)}$ is the Algebraic model solution (Eq. (9)), C_n are the polynomial coefficients, and with $A^{(kn)}$ given in Table 1 for N up to 10th degree. The $A^{(k)}$ coefficients are obtained after k times differentiation of the exponential solution as in Eq. (16), then setting $\alpha = 0$, introducing the ζ_c, λ and ω transformations, and factoring like terms in Eq. (12). The process is illustrated in Appendix A.

It is worth noting that the general solution $\theta_f^{exp}(\tau,\zeta,\alpha)$ can be used to explore initial conditions given as Fourier series. For this, one needs general solutions $\theta_{f,IC}^{F,c}(\zeta,\alpha) = \cos(\alpha\zeta)$ and $\theta_{f,IC}^{F,s}(\zeta,\alpha) = \sin(\alpha\zeta)$, which are formally obtained from $\theta_f^{exp}(\tau,\zeta,\alpha)$ in a straightforward way, see Appendix B.

2.3. Thermal losses through tank walls

The thermocline tank problem as solved above neglects thermal losses through the tank walls to the environment. Herein we also consider these thermal losses by addressing Eq. (1) in full, in particular including the energy sink term $h_w A_w(T_{amb} - T_f)$, representing the heat losses (see also Esence et al. (2017) for full equations). In the dimensionless form of Eq. (7), this energy sink would be expressed as $\mathrm{Bi}_w(\theta_{amb} - \theta_f)$, with

$$\mathrm{Bi}_w = \mathrm{Bi}\frac{h_w A_w}{h_{sf} A_{sf}}, \tag{19}$$

where h_w is the wall heat transfer coefficient and A_w is the tank wall-surface area per volume. For a cylindrical tank of radius R transferring heat only through its side walls to the environment, we obtain $A_w = 2/R$.

To formally obtain the one-dimensional equations governing the thermocline tank, we need assert that the assumptions for one-dimensionality still hold, namely that there is no angular dependence of temperature at each tank location and that the boundary layer on the tank walls is thin, allowing for $\theta_f = \theta_s$ on the wall. Further, the wall heat capacity is negligible compared to that of the fluid and solid, negating the need for solving a coupled equation for the wall temperature as given in Esence et al. (2017). The latter condition may be verified by establishing that the fluid-solid heat transfer coefficient and the advection are both much faster than the wall heat transfer, e.g. by verifying that $\mathrm{Bi}_w \ll \mathrm{Bi}$ and $\mathrm{Bi}_w \ll (\gamma_{f|s}\mathrm{Pe})$.

Including the thermal losses from the wall, the solution for the fluid temperature becomes

$$\theta_f(\tau,\zeta) = \exp(-\mathrm{Bi}_w\tau)(\theta - \theta_{amb}) + \theta_{amb} \tag{20}$$

where θ is the fluid temperature without considering heat losses, ob-

Table 1
Coefficients $A^{(kn)}$ for the Algebraic Model with polynomial initial condition.

cline2-12 N	0	1	2	3	4	5	6	7	8	9	10
0	1										
1	1	2									
2	2	2	4								
3	4	12	4	8							
4	12	20	48	8	16						
5	32	120	72	160	16	32					
6	120	264	720	224	480	32	64				
7	384	1680	1392	3360	640	1344	64	128			
8	1680	4464	13440	5920	13440	1728	3584	128	256		
9	6144	30,240	31,200	80,640	22,080	48,384	4480	9216	256	512	
10	30240	92,640	302,400	168,960	403,200	75,264	16,1280	11,264	23,040	512	1024

tained either from the Algebraic (Eq. (9)) or the Algebraic IC (Eq. (18)) model.

3. Model validation

3.1. Temperature profiles

As validation, and to verify the accuracy of the Algebraic IC model, we compare temperature profiles against those obtained from the recent experimental campaign of Hoffmann et al. (2016), and specifically their Fig. 5, where profiles for a thermocline discharge cycle are presented. Relevant geometry, material and operating properties are given in Table 2. All measurements have been made dimensionless through the scaling factors in Eq. (5) to conform with the notation of the present article. The solid and fluid thermo-physical properties have been evaluated at the average temperature between hot and cold.

The initial profile given by Hoffmann was fit with a 4th degree polynomial, and the additional constraint that $\partial\theta/\partial\zeta = 0$ at $\zeta=1$ was imposed when determining the polynomial coefficients. Further, the Algebraic Model (e.g. with a step initial profile) and the solution from the numerical integration of Eq. (8) starting with the same polynomial expression for the initial temperature profile is evaluated, with results presented in Fig. 2.

From consideration of the results, the following conclusions may be drawn:

- Both the Algebraic and Algebraic IC models predict well the behavior of the thermocline. As time progresses, the two models tend to the same solution, since they are both based on the exact solution for a semi-infinite domain ($L\to\infty$).
- Using the polynomial initial condition allows for a closer match of the initial profiles with the experimental data. This highlights the importance of capturing correctly the initial temperature distribution of the thermocline tank, which will result in a more accurate prediction of thermocline location and thickness.
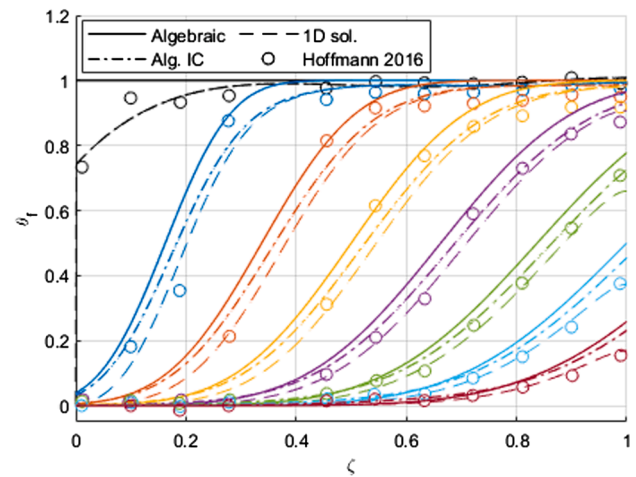
Fig. 2. Temperature profiles during a discharge cycle as predicted by the Algebraic, Algebraic IC (Alg. IC) and 1D numerical (1D sol) models, and compared to experimental results from Hoffmann et al. (2016)).

- The numerical solution has a superior performance to both algebraic models. This is expected for the particular set of experimental conditions because the algebraic solutions were developed for "steep" profiles, e.g. for $D^\star/u^\star \ll 1$ (Votyakov and Bonanos, 2015).

3.2. Tank exit temperature

In Fig. 3, the thermocline tank exit temperature is plotted as a function of dimensional time in hours, as predicted by the models discussed herein and compared to experimental results from Hoffmann et al. (2016). Two features are evident from considering the experimental data: initially (up to the ~2 hour mark), a small decrease in tank exit temperature is observed due to heat losses to the environment. Subsequently, once the thermocline begins to exit the tank, the temperature decrease becomes much more rapid.

Six additional curves are superimposed onto the experimental data, those for the Algebraic, Algebraic IC and 1D solutions, with (dashed lines) and without (solid lines) heat losses. When heat losses are not considered, the initial gradual temperature decrease is not captured, as expected. Both the Algebraic and Algebraic IC models capture the decay of the exit temperature during the discharge cycle, with the Algebraic IC
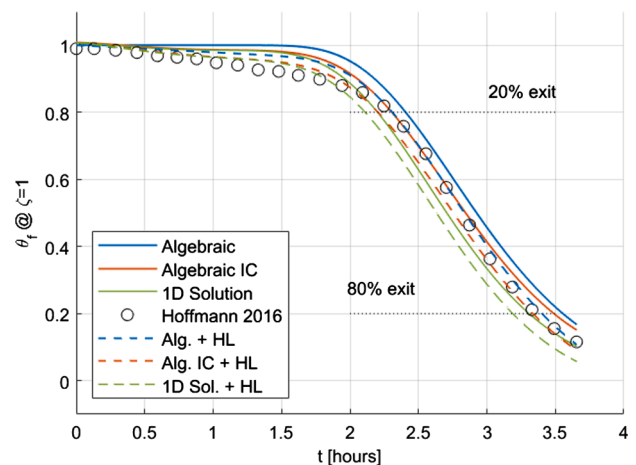
Table 2

Relevant properties of thermocline presented in Hoffmann et al. (2016), along with calculated dimensionless parameters.

Tank geometry	
Tank height, L	1.8 [m]
Tank diameter	0.4 [m]
Particle diameter, d_p	40 [mm]
Porosity, ε	0.41
Operating conditions	
Hot Temperature, T_{in}	210 [°C]
Cold Temperature, T_∞	160 [°C]
Charge time, t	3.0 [h]
Material properties at mean temp., $(T_{in} + T_\infty)/2$	
Fluid thermal conductivity, k_f	0.208 [W/m K]
Fluid density, ρ_f	804 [kg/m³]
Fluid heat capacity, $C_{p,f}$	2472 [J/kg K]
Fluid viscosity, μ_f	$4 \cdot 10^{-3}$ [Pa·s]
Solid thermal conductivity, k_s	5.69 [W/m K]
Solid density, ρ_s	2500 [kg/m³]
Solid heat capacity, $C_{p,s}$	830 [J/kg K]
Calculated dimensionless properties	
γ_f	0.4
β_f	0.025
$u^\star$	177.73
$D^\star$	4.84
Pe	444.63
Bi	2695.64

Fig. 3. Thermocline tank exit temperature as a function of time, as predicted by the Algebraic, Algebraic IC and 1D numerical solutions, and compared to experimental results from Hoffmann et al. (2016). Dashed lines represent solutions including heat losses to the environment. The temperature when a particular fraction of the thermocline has exited the tank is also indicated.

model better fitting the data. Interestingly, the 1D solution predicts a lower exit temperature at each time. This is attributed to the boundary condition imposed, namely that $\partial\theta/\partial\zeta=0$ at $\zeta=1$ (also observed in the temperature profiles in Fig. 2), which is necessary for full specification of the governing PDE. The same trends are observed for the solutions including heat losses. Note that in this work the dimensionless heat transfer coefficient has been guessed and a value of 3 was found to suitably fit the data - for a predictive correlation the reader is referred to Hoffmann et al. (2016).

3.3. Algebraic IC model validation

The claim was made that the Algebraic IC and 1D solutions do not precisely coincide in Fig. 2 because of the specific $D^\star/u^\star$ value of the reference problem of Hoffmann et al. (2016). To demonstrate this, the same properties as listed in Table 2 are used, but an arbitrary $D^\star$ is used to obtain $2.5\cdot10^{-2}\leqslant D^\star/u^\star\leqslant2.5\cdot10^{-3}$, where again $2.5\cdot10^{-2}$ is the value from Table 2. The predictions of the Algebraic IC model are compared to the 1D numerical solution, as shown in Fig. 4, where it is clearly seen that as the ratio of $D^\star/u^\star$ decreases, e.g. the thermocline becomes steeper, the agreement between the two models improves to the point where the solutions become indistinguishable.

However, despite the apparent discrepancy in the fluid temperature distribution between the numerical solution and the Algebraic IC model, the parameter of interest to the thermocline storage tank designer or plant operator is the thermocline thickness, which herein is defined as the inverse of the maximum slope of θ_f (c.f. Section 4.3). According to this metric, the discrepancy between the two models is less than 5% by the end of the charge/discharge cycle for $D^\star/u^\star = 2.5\cdot10^{-2}$, reducing to a perfect agreement as the ratio decreases.

4. Thermocline tank operating characteristics

4.1. Effect of thermal losses

The new Algebraic IC model allows for exploring the impact of thermal losses from the thermocline tank walls to the environment. In Fig. 5, the thermocline tank exit temperature for the tank of Table 2 is investigated under different dimensionless heat transfer coefficients. The ambient temperature is assumed to be 25 °C, corresponding to $\theta_{amb} = -2.7$. Two effects are discernible: as mentioned earlier, in the time before the thermocline exits the tank, e.g. before ~2 h, a larger Bi_w leads to a steeper decrease in exit temperature, as the temperature of the hot fluid within the tank decreases because of the thermal losses.

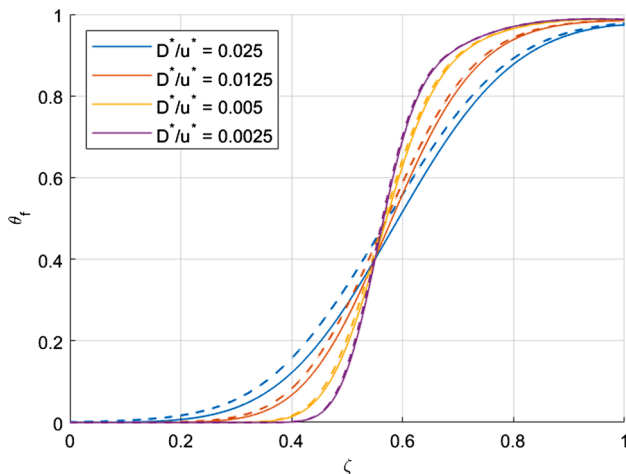A secondary effect is the decrease in final tank temperature at the end

Fig. 4. Fluid temperature profiles for various $D^\star/u^\star$ ratios, as predicted by the 1D solution (solid lines) and the Algebraic IC model (dashed lines).
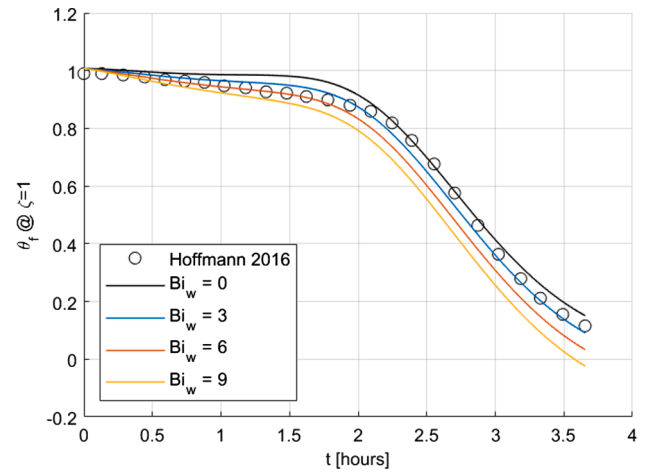

Fig. 5. Effect of dimensionless heat transfer coefficient, Bi_w, on tank exit temperature.

of the discharge process, e.g. at 3.5 hours. In the limit of a perfectly insulated tank ($Bi_w=0$), when the thermocline exits completely the tank the final temperature will reach the cold fluid temperature (here noted as $\theta_\infty = 0$). However, in a tank with thermal losses, the temperature approached would be that of the ambient conditions, since $\theta_{amb} < \theta_\infty$.

4.2. Effect of fluid velocity

In order to ascertain the effect of fluid velocity, its impact on the thermocline tank efficiency is studied. The thermocline thickness, λ, may be used as a proxy to the tank efficiency (Bonanos and Votyakov, 2016):

$$\eta = 1 - \frac{\lambda}{2}. \tag{21}$$

However, as noted elsewhere (Bonanos and Votyakov, 2016), the thermocline thickness at any time $\tau = \zeta/u^\star$ is inversely proportional to the maximum slope of the thermocline, e.g. $\lambda = 1/\max(\partial\theta_f/\partial\zeta)$.

The existence of an optimal fluid velocity, leading to the minimum thermocline thickness for a particular configuration, has been argued previously (Yang and Garimella, 2010; Votyakov and Bonanos, 2015). The analytic expression for $D^\star$ allows to explicitly predict the optimal fluid velocity without multiple simulations: instead it can be obtained by minimizing $D^\star/u^\star$ by solving $\partial(D^\star/u^\star)/\partial u^\star = 0$. The result is given in terms of the optimal Peclet number, $Pe^\star$:

$$Pe^\star = \frac{\sqrt{Bi}}{\gamma_s\gamma_f}. \tag{22}$$

To demonstrate the accuracy of this solution, a parametric analysis of the thermocline tank was performed, varying the tank discharge time from 1 to 20 h, and the porosity from 0.1 and 0.9, as shown in Fig. 6. Note that fluid velocity and discharge time are inversely proportional, since $u = L\varepsilon/(\gamma_f t)$, e.g. for the same tank, a longer characteristic time implies a slower moving fluid. For the present results, a uniform initial tank temperature was assumed with negligible thermal losses. Superimposed on this is the solution for the optimal discharging velocity, $Pe^\star$, which indeed predicts the minimum thermocline thickness. The thermocline thickness was established at 50% thermocline extraction.

Aside from the guidance provided to thermocline tank designers regarding fluid velocity through $Pe^\star$, the speed of the Algebraic solutions expedites the exploration of the full parametric space, allowing for trade-offs to be visualized without requiring computationally intensive solutions.
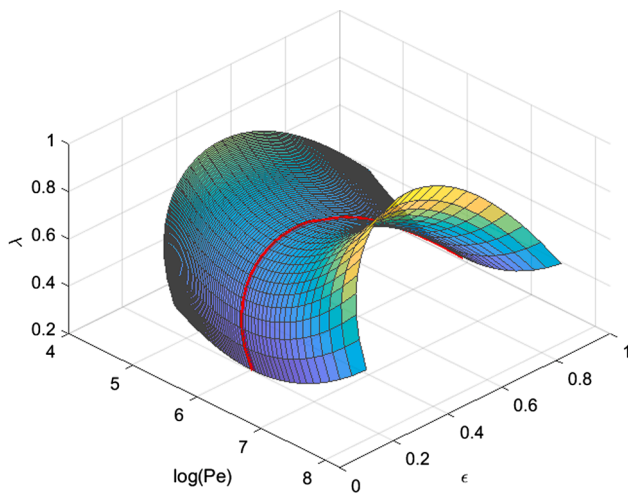
Fig. 6. Surface plot of thermocline thickness at the end of the discharge cycle ($\tau = \zeta u^\star$) as a function of porosity (ε) and fluid velocity (expressed through Pe).

4.3. Multiple-cycle operation

A typical thermocline tank integrated in a concentrated solar thermal power plant undergoes consecutive charging and discharging cycles over the daily cycle. Depending on the operational strategy, full or partial extraction of the thermocline will occur after each cycle. This, in turn, means that each consecutive cycle would not start from a uniform tank temperature, but rather from some other temperature profile. Therefore, the mathematical framework developed herein is ideally suited to investigate the performance of thermocline tanks under multiple consecutive cycle operation.

In the present example, the thermocline tank geometry, material and flow characteristics are as described in Table 2, the tank was initialized with a uniform "hot" temperature ($\theta_f(0,\zeta) = 1$), and no heat losses to the environment were considered. Each cycle was stopped when a predefined fraction of the thermocline exited the tank, or in other words when the exit temperature reached a set vale, for example if 80% of the thermocline exited, then $\theta_f(\tau,1)=0.2$ (c.f. Fig. 3). Further, we assume that there is no thermocline degradation in periods when the tank is idle, e.g. when there is no charging or discharging occurring.

The tank efficiency was calculated and plotted over a number of cycles, as shown in Fig. 7, where it is evident that multiple cycle operation leads to an asymptotic decay in tank efficiency. We note that
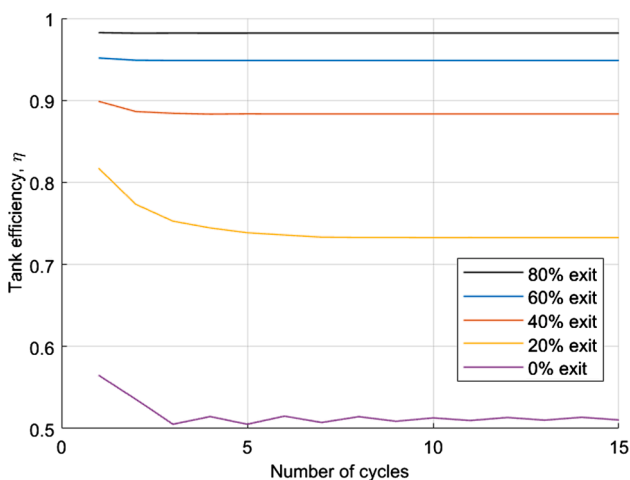

Fig. 7. Evolution of tank efficiency over multiple charge and discharge cycles, as a function of percentage of thermocline exiting the tank.

independent of the thermocline thickness allowed to exit the tank, steady-state in tank efficiency is reached in under 10 cycles. Physically, each cycle starts with some non-uniform temperature distribution, governed by the amount of thermocline allowed to exit in the previous cycle. Therefore, less volume is available to store (or deliver) energy, reducing the effective tank capacity with each cycle. This leads to the observed decrease in tank efficiency with the number of cycles. An additional effect is that the charge/discharge time of the tank also decreases with the number of cycles: since less useful volume is available, it will charge (or discharge) in less time, since, as the flow conditions are the same, the thermocline front is also advected with the same velocity. Note that in the case that the thermocline is not allowed to exit the tank (0% exit in Fig. 7), the fundamental limit of 50% tank efficiency is reached, since the thermocline zone spans the entire height of the storage tank.

5. Summary and conclusions

In the present study, the algebraic model developed by the authors (Votyakov and Bonanos, 2014; Votyakov and Bonanos, 2015) was extended to accommodate non-uniform temperature initial conditions. The new model, called the Algebraic IC model, can handle initial temperature distributions described by a polynomial function, as polynomials of sufficiently large degree can accurately fit almost all experimental profiles found in the literature. The coefficients required for the solution are supplied for up to 10th degree polynomials. Additionally, the solution including thermal losses from the thermocline tank wall to the environment is provided. The developed framework allows for multiple consecutive charge and discharge cycles to be simulated.

The Algebraic IC model is validated by comparing the solution to experimental data by Hoffmann et al. (2016) and with the solution obtained through numerical integration of the governing differential equations for conservation of energy. Although the Algebraic model was developed for $D^\star/u^\star \ll 1$ (e.g. "steep" thermoclines), its performance is still very good even when this constraint is not strictly adhered to, as demonstrated through comparison with the aforementioned experimental study. However, even when the $D^\star/u^\star$ constraint is not strictly valid, the thermocline thickness at the end of the charge or discharge cycle is under-predicted by less than 5%.

Incorporation of thermal losses from the thermocline tank side walls to the ambient temperature leads to capturing the gradual decrease of fluid exit temperature from the tank before the thermoclien exits, but also to a temperature lower than the fluid "cold" temperature at the end of the charge/discharge cycle, as energy is lost to the environment.

While considering the effect of fluid velocity on the thermocline thickness, results show that an optimum charging velocity exists, which results in a minimum thermocline thickness within the tank. An explicit formula for the calculation of this optimal velocity is given as Pe*. This is a new result arising from the algebraic model that was not previously captured by the one-phase models currently used in the literature.

The tank was further simulated over multiple charging and discharging cycles. A decay in tank efficiency was observed, which however depends on the fraction of the thermocline that is allowed to exit the tank. In all cases, a steady state was achieved in the particular tank considered in under 10 cycles. Further, the more the thermocline was allowed to exit, the higher the tank efficiency.

Declaration of Competing Interest

The authors declare that they have no known competing financial interests or personal relationships that could have appeared to influence the work reported in this paper.

Appendix A. Coefficients $A^{(kn)}$

For each calculation, the initial point is Eq. (16). Srart with $n = 0$:

$$\theta_f^{(0)}(\tau,\zeta) = \theta_f^{exp}(\tau,\zeta,0) \tag{A.1}$$

$$= \frac{1}{2}\left\{1 + \text{erf}\left[\frac{\zeta - u\tau}{\sqrt{4D\tau}} + \alpha\sqrt{D\tau}\right]\right\}e^{\alpha(\zeta - u\tau) + \alpha^2 D\tau}\Bigg|_{\alpha=0} \tag{A.2}$$

$$= \frac{1}{2}\left\{1 + \text{erf}(\omega)\right\} \tag{A.3}$$

$$= \text{EF}(\omega) \tag{A.4}$$

Thus, $A^{(00)} = 1$. Note, the trivial step function charge and discharge case is controlled by C_0, i.e. $C_0 = 0$ for discharge and $C_0 = 1$ for charge.

For $n = 1$ differentiate $\theta_f^{exp}(\tau,\zeta,\alpha)$ and then set $\alpha = 0$:

$$\theta_f^{(1)}(\tau,\zeta) = \frac{\partial \theta_f^{exp}(\tau,\zeta,\alpha)}{\partial \alpha}\Bigg|_{\alpha=0} \tag{A.5}$$

$$\frac{\partial \theta_f^{exp}(\tau,\zeta,\alpha)}{\partial \alpha} = e^{\frac{\alpha^2\lambda^2}{4} + \alpha\lambda\omega}\left(\frac{\alpha\lambda^2}{2} + \lambda\omega\right)\frac{1}{2}\left[\text{erf}\left(\frac{\alpha\lambda}{2} + \omega\right) + 1\right] + \frac{\lambda e^{-\omega^2}}{2\sqrt{\pi}} \tag{A.6}$$

$$\frac{\partial \theta_f^{exp}(\tau,\zeta,\alpha)}{\partial \alpha}\Bigg|_{\alpha=0} = \frac{\lambda}{2}\left\{\text{GF}(\omega) + 2\omega\text{EF}(\omega)\right\} \tag{A.7}$$

This corresponds to the $N = 1$ row of Table 1, where for $k = 0$ (even case), the coefficient of the $\text{EF}(\omega)$ term is 1, while for $k = 1$ (odd case), the coefficient of the $\text{GF}(\omega)$ term is 2.

For $n = 2$ differentiate $\theta_f^{exp}(\tau,\zeta,\alpha)$ two times and then set $\alpha = 0$:

$$\theta_f^{(2)}(\tau,\zeta) = \frac{\partial^2 \theta_f^{exp}(\tau,\zeta,\alpha)}{\partial \alpha^2}\Bigg|_{\alpha=0} \tag{A.8}$$

$$\frac{\partial^2 \theta_f^{exp}(\tau,\zeta,\alpha)}{\partial \alpha^2} = \frac{\lambda^2 e^{-\omega^2}}{4}\frac{(\alpha\lambda + 2\omega)}{\sqrt{\pi}}$$
$$+ \frac{\lambda^2 e^{-\omega^2}}{8}e^{\left(\frac{\alpha\lambda}{2} + \omega\right)^2}\left((\alpha\lambda + 2\omega)^2 + 2\right)\left[1 + \text{erf}\left(\frac{\alpha\lambda}{2} + \omega\right)\right] \tag{A.9}$$

$$\frac{\partial^2 \theta_f^{exp}(\tau,\zeta,\alpha)}{\partial \alpha^2}\Bigg|_{\alpha=0} = \frac{\lambda^2}{4}\left\{2\text{EF}(\omega) + 2\omega\text{GF}(\omega) + 4\omega^2\text{EF}(\omega)\right\} \tag{A.10}$$

Again, this corresponds to the $N = 2$ row of Table 1. For $k = 0$ the coefficient of $\text{EF}(\omega)$ term is 2, for $k = 1$ the coefficient of $\text{GF}(\omega)$ term is 2, and $k = 2$, the coefficient of $\text{EF}(\omega)$ term is 4.

The above symbolic calculations are cumbersome, but they can be conveniently performed in Wolfram Mathematica for any order of derivatives.

Appendix B. Initial condition as Fourier expansion

Arbitrary initial condition can be represented as Fourier series. Fourier terms of the series, $\theta_{f,IC}^{F,c}(\zeta,\alpha) = \cos(\alpha\zeta)$ and $\theta_{f,IC}^{F,s}(\zeta,\alpha) = \sin(\alpha\zeta)$, are obtained in straightforward way:

$$\theta_f^{F,c}(\tau,\zeta,\alpha) = \frac{1}{2}\left[\theta_f^{exp}(\tau,\zeta,i\alpha) + \theta_f^{exp}(\tau,\zeta,-i\alpha)\right], \tag{B.1}$$

$$\theta_f^{F,s}(\tau,\zeta,\alpha) = \frac{1}{2i}\left[\theta_f^{exp}(\tau,\zeta,i\alpha) - \theta_f^{exp}(\tau,\zeta,-i\alpha)\right]. \tag{B.2}$$

These formulas require calculus of the error function with complex variable, which is more difficult to deal with compared to the polynomial terms.

Appendix C. Supplementary material

Supplementary data associated with this article can be found, in the online version, at https://doi.org/10.1016/j.solener.2020.11.011.

References

Amiri, A., Vafai, K., 1994. Analysis of dispersion effects and non-thermal equilibrium, non-darcian, variable porosity incompressible flow through porous media. Int. J. Heat Mass Transf. 37 (6), 939–954.

Bayon, R., Rojas, E., 2013. Simulation of thermocline storage for solar thermal power plants: from dimensionless results to prototypes and real-size tanks. Int. J. Heat Mass Transf. 60, 713–721.

Bayon, R., Rojas, E., 2018. Analysis of packed-bed thermocline storage tank performance by means of a new analytical function. In: AIP Conf. Proc., 2033. https://doi.org/10.1063/1.5067096.

Biencinto, M., Bayon, R., Rojas, E., Gonzalez, L., 2014. Simulation and assessment of operation strategies for solar thermal power plants with a thermocline storage tank. Sol. Energy 103, 456–472. https://doi.org/10.1016/j.solener.2014.02.037.

Bonanos, A.M., Votyakov, E.V., 2016. Sensitivity analysis for thermocline thermal storage tank design. Renewable Energy 99, 764–771. https://doi.org/10.1016/j.renene.2016.07.052. ISSN 0960-1481.

Bruch, A., Fourmigue, J.F., Couturier, R., 2014. Experimental and numerical investigation of a pilot-scale thermal oil packed bed thermal storage system for csp power plant. Sol. Energy 105, 116–125. https://doi.org/10.1016/j.solener.2014.03.019.

Esence, T., Bruch, A., Molina, S., Stutz, B., Fourmigue, J.F., 2017. A review on experience feedback and numerical modeling of packed-bed thermal energy storage systems. Sol. Energy 153, 628–654. https://doi.org/10.1016/j.solener.2017.03.032.

Faas, S.E., Thorne, L.R., Fuchs, E.A., Gilbertsen, N.D., 1986. 10mwe solar athermal central receiver plant: Thermal storage subsystem evaluation – final report. techreport SAND86-8212, Sandia National Laboratories.

Flueckiger, S., Yang, Z., Garimella, S.V., 2011. An integrated thermal and mechanical investigation of molten-salt thermocline energy storage. Appl. Energy 88 (6), 2098–2105. https://doi.org/10.1016/j.apenergy.2010.12.031.

Flueckiger, S.M., Garimella, S.V., 2012. Second-law analysis of molten-salt thermal energy storage in thermoclines. Sol. Energy 86 (5), 1621–1631.

Flueckiger, S.M., Yang, Z., Garimella, S.V., 2013. Review of molten-salt thermocline tank modeling for solar thermal energy storage. Heat Transfer Eng. 34 (10), 787–800.

Hänchen, M., Brückner, S., Steinfeld, A., 2011. High-temperature thermal storage using a packed bed of rocks e heat transfer analysis and experimental validation. Appl. Therm. Eng. 31, 1798–1806.

Hoffmann, J.F., Fasquelle, T., Goetz, V., Py, X., 2016. A thermocline thermal energy storage system with filler materials for concentrated solar power plants: experimental data and numerical model sensitivity to different experimental tank scales. Appl. Therm. Eng. 100, 753–761. https://doi.org/10.1016/j.applthermaleng.2016.01.110.

Kuravi, S., Trahan, J., Goswami, D.Y., Rahman, M.M., Stefanakos, E.K., 2013. Thermal energy storage technologies and systems for concentrating solar power plants. Prog. Energy Combust. Sci. 39 (4), 285–319. https://doi.org/10.1016/j.pecs.2013.02.001. ISSN 0360–1285.

Kuznetsov, A.V., 1995. An analytical solution for heating a two-dimensional porous packed bed by a non-thermal equilibrium fluid flow. Appl. Sci. Res. 55, 83–93.

Van Lew, J.T., Li, P., Chan, C.L., Karaki, W., Stephens, J., 2011. Analysis of heat storage and delivery of a thermocline tank having solid filler material. J. Sol.Energy Eng. 133 (2), 021003.

Pacheco, J.E., Showalter, S.K., Kolb, W.J., 2002. Development of a molten-salt thermocline thermal storage system for parabolic trough plants. J. Sol. Energy Eng. 124 (2), 153–159.

Vafai, K., Sozen, M., 1990. Analysis of energy and momentum transport for fluid flow through a porous bed. J. Heat Transfer 112 (3), 690–699.

Votyakov, E.V., Bonanos, A.M., August 2014. A perturbation model for stratified thermal energy storage tanks. Int. J. Heat Mass Transf. 75, 218–223.

Votyakov, E.V., Bonanos, A.M., 2015. Algebraic model for thermocline thermal storage tank with filler material. Sol. Energy 122, 1154–1157.

Wakao, N., Funazkri, T., 1978. Effect of fluid dispersion coefficients on particle-to-fluid mass transfer coefficients in packed beds: correlation of sherwood numbers. Chem. Eng. Sci. 33 (10), 1375–1384.

Wakao, N., Kaguei, S., Funazkri, T., 1979. Effect of fluid dispersion coefficients on particle-to-fluid heat transfer coefficients in packed beds: correlation of nusselt numbers. Chem. Eng. Sci. 34 (3), 325–336.

Wang, G., Yu, S., Niu, S., Chen, Z., Hu, P., 2020. A comprehensive parametric study on integrated thermal and mechanical performances of molten-salt-based thermocline tank. Appl. Therm. Eng. 170, 115010. https://doi.org/10.1016/j.applthermaleng.2020.115010.

Xu, B., Li, P., Chan, C.L., 2012. Extending the validity of lumped capacitance method for large biot number in thermal storage application. Sol. Energy 86 (6), 1709–1724.

Xu, C., Wang, Z., He, Y., Li, X., Bai, F., 2012. Sensitivity analysis of the numerical study on the thermal performance of a packed-bed molten salt thermocline thermal storage system. Appl. Energy 92, 65–75.

Yang, Z., Garimella, S.V., 2010. Thermal analysis of solar thermal energy storage in a molten-salt thermocline. Sol. Energy 84 (6), 974–985.